Geophys. J. Int. (2007) doi: 10.1111/j.1365-246X.2007.03474.x

First-order *P*-wave ray synthetic seismograms in inhomogeneous weakly anisotropic media

Ivan Pšenčík[1] and Véronique Farra[2]

[1] *Geophysical Institute, Acad. Sci. of Czech Republic, Boční II,* 141 31 *Praha* 4*, Czech Republic. E-mail: ip@ig.cas.cz*
[2] *Institut de Physique du Globe de Paris,* 4 *Place Jussieu,* 75252 *Paris Cedex* 05, *France. E-mail: farra@ipgp.jussieu.fr*

Accepted 2007 April 23. Received 2007 April 12; in original form 2006 November 29

SUMMARY

We propose approximate equations for *P*-wave ray theory Green's function for smooth inhomogeneous weakly anisotropic media. Equations are based on perturbation theory, in which deviations of anisotropy from isotropy are considered to be the first-order quantities. For evaluation of the approximate Green's function, earlier derived first-order ray tracing equations and in this paper derived first-order dynamic ray tracing equations are used.

The first-order ray theory *P*-wave Green's function for inhomogeneous, weakly anisotropic media of arbitrary symmetry depends, at most, on 15 weak-anisotropy parameters. For anisotropic media of higher-symmetry than monoclinic, all equations involved differ only slightly from the corresponding equations for isotropic media. For vanishing anisotropy, the equations reduce to equations for computation of standard ray theory Green's function for isotropic media. These properties make the proposed approximate Green's function an easy and natural substitute of traditional Green's function for isotropic media.

Numerical tests for configuration and models used in seismic prospecting indicate negligible dependence of accuracy of the approximate Green's function on inhomogeneity of the medium. Accuracy depends more strongly on strength of anisotropy in general and on angular variation of phase velocity due to anisotropy in particular. For example, for anisotropy of about 8 per cent, considered in the examples presented, the relative errors of the geometrical spreading are usually under 1 per cent; for anisotropy of about 20 per cent, however, they may locally reach as much as 20 per cent.

Key words: inhomogeneous media, *P* waves, perturbation methods, seismic anisotropy, seismic ray theory, synthetic seismograms.

1 INTRODUCTION

We extend the applicability of the procedure for an approximate *P*-wave ray tracing and ray theory traveltime computations in smooth laterally inhomogeneous, weakly anisotropic media, proposed by Pšenčík & Farra (2005) and called first-order ray tracing (FORT), to computations of *P*-wave ray amplitudes and ray theory Green's function. In this way, approximate *P*-wave ray theory synthetic seismograms in smooth inhomogeneous weakly anisotropic media can be computed very efficiently. The extension depends basically on the first-order dynamic ray tracing (FODRT). The FODRT equations depend, as the FORT equations do, on only 15 weak-anisotropy (WA) parameters, which depend on all 21 elastic moduli, or some of their combinations. The WA parameters represent a linearized generalization, to weakly anisotropic media of arbitrary symmetry, of Thomsen's (1986) parameters for transversely isotropic media, see Appendix A and Pšenčík & Gajewski (1998) or Farra & Pšenčík (2003).

Presented results are based on perturbation theory, in which small deviations of anisotropy from isotropy are considered to be of the first order. As in the case of the kinematic ray tracing, the approximate dynamic ray tracing equations are derived from the exact ones so that the exact eigenvalue of the Christoffel matrix, appearing in them, is substituted by its first-order approximation. This is why we speak about FORT and FODRT. FORT and FODRT do not require calculation of reference rays in a reference medium as is common in most perturbation approaches. FORT and FODRT are used just for the given weakly anisotropic medium. They provide directly the first-order rays, the first-order or second-order traveltimes and first-order ray amplitudes along them. FORT and FODRT are very simple and transparent. They provide simplified relations between ray attributes and model parameters. Another useful property is that FORT and FODRT provide description of *P*-wave propagation decoupled from *S*-wave propagation. For anisotropic media of higher symmetry than monoclinic, FORT and FODRT differ only slightly from their isotropic counterparts used in many routine applications. This makes FORT and FODRT their natural potential substitutes.

A brief review of FORT in the next section is followed by a section, in which formulae for the first-order ray theory Green's function and related first-order quantities, on which it depends, are

presented. Basic role is played by FODRT. The final sections are devoted to numerical examples illustrating the accuracy of the proposed approach and to conclusions. Appendix A contains definitions of the *P*-wave WA parameters. Appendix B contains explicit expressions for the first and second derivatives of the first-order *P*-wave eigenvalue with respect to spatial coordinates and with respect to components of the slowness vector. The expressions are valid for inhomogeneous media of weak, but arbitrary anisotropy.

Three quantities with dimension of wave velocity are used in the text: c, α and V_P. The symbol c denotes spatially and angularly varying *P*-wave phase velocity. The symbol α denotes the *P*-wave velocity of a reference isotropic medium. The velocity α is an arbitrary constant; it is used for the definition of the WA parameters, see Appendix A. If elastic parameters were used instead of WA parameters, the symbol α would disappear from the RT and DRT equations. Finally, the velocity V_P is the *P*-wave velocity of a reference isotropic medium varying along a ray, along which the evaluation of the second-order traveltime correction is performed.

In the following, component notation is mostly used. Einstein summation convention is used for the repeated subscripts. Subscripts behind a comma denote differentiation with respect to the corresponding Cartesian coordinates. Lower-case indices run from 1 to 3, the upper-case indices from 1 to 2.

2 FORMULAE FOR THE *P*-WAVE FIRST-ORDER RAY TRACING

Explicit expressions of the *P*-wave FORT equations for inhomogeneous media of weak, but arbitrary anisotropy can be found in Pšenčík & Farra (2005), where also specifications for selected media of higher symmetry than monoclinic are given. Formally, FORT equations can be written as follows:

$$\frac{dx_i}{d\tau} = \frac{1}{2}\frac{\partial G}{\partial p_i}, \qquad \frac{dp_i}{d\tau} = -\frac{1}{2}\frac{\partial G}{\partial x_i}. \tag{1}$$

Here x_i are Cartesian coordinates of the trajectory of the first-order ray, and p_i are components of the first-order slowness vectors at corresponding points of the ray, $p_i = n_i/c$. The vector $\mathbf{n}$ is the unit normal to the wave front (the unit vector parallel to the slowness vector $\mathbf{p}$) and $c = c(x_m, n_m)$ is the first-order phase velocity. The parameter along the ray, τ, in eq. (1) is the first-order traveltime. The symbol $G = G(x_m, p_m)$ denotes the greatest of the three first-order eigenvalues of the generalized Christoffel matrix:

$$\Gamma_{ik}(x_m, p_m) = a_{ijkl}(x_m) p_j\, p_l. \tag{2}$$

The matrix Γ_{ik} is called generalized since it depends on p_i instead on n_i, which appear in the classical Christoffel matrix, $\bar{\Gamma}_{ik} = a_{ijkl} n_j n_l$. For simplicity, we call Γ_{ik} from eq. (2) the Christoffel matrix in the following text. The symbol a_{ijkl} in eq. (2) denotes the tensor of density-normalized elastic moduli.

The slowness vectors determined from eq. (1) have to satisfy, at each point of the ray, the first-order eikonal equation:

$$G(x_m, p_m) = \Gamma_{ik}(x_m, p_m) n_i\, n_k = c^{-2} G(x_m, n_m) = 1, \tag{3}$$

where c denotes again the first-order phase velocity of the considered *P* wave. The first-order *P*-wave eigenvalue $G(x_m, p_m)$ of the Christoffel matrix is given by an explicit formula (Pšenčík & Farra 2005):

$$\begin{aligned} G(x_m, p_m) = \alpha^2 \big\{ & p_k p_k + 2\big(\epsilon_x p_1^2 + \epsilon_y p_2^2 + \epsilon_z p_3^2\big) \\ & + 2(p_k p_k)^{-1}\big[\eta_x p_2^2 p_3^2 + \eta_y p_1^2 p_3^2 + \eta_z p_1^2 p_2^2 \\ & + 2(\epsilon_{16} p_2 + \epsilon_{15} p_3) p_1^3 + 2(\epsilon_{24} p_3 + \epsilon_{26} p_1) p_2^3 \\ & + 2(\epsilon_{35} p_1 + \epsilon_{34} p_2) p_3^3 \\ & + 2(\chi_x p_1 + \chi_y p_2 + \chi_z p_3) p_1 p_2 p_3\big]\big\}. \end{aligned} \tag{4}$$

The definition of the WA parameters acting as coefficients in eq. (4) is given in (A1). The parameters η_x, η_y and η_z are defined in eq. (A2). The quantity α in eq. (4) is a reference velocity used in the definition of WA parameters, see eq. (A1). By inserting (A1) into (4), it can be easily shown that $G(x_m, p_m)$ and its derivatives are independent of α, see Pšenčík & Farra (2005). The reference velocity α can thus be chosen as an arbitrary non-zero constant ($\alpha \neq 0$), which can be chosen, for example, so that it makes the WA parameters as small as possible.

The explicit expressions for the FORT in an inhomogeneous weakly anisotropic medium as well as for several weakly anisotropic media of higher symmetry than monoclinic can be found in Pšenčík & Farra (2005). The expressions for the derivatives $\partial G/\partial x_i$ and $\partial G/\partial p_i$ appearing in eq. (1) can be found in Appendix B, see eq. (B1).

The initial conditions at the source, for $\tau = 0$, read:

$$x_i(0) = x_i^0, \qquad p_i(0) = p_i^0. \tag{5}$$

Here x_i^0 are the coordinates of the source point and p_i^0 are the components of the first-order slowness vector, specified as $p_i^0 = n_i^0/c_0$. The symbol c_0 denotes the first-order approximation of the phase velocity in the direction specified by the vector $\mathbf{n^0}$ at the point with coordinates x_i^0. The phase velocity c_0 is given by the square root of $G(x_m^0, n_m^0)$, see eqs (3) and (5). The vector $\mathbf{n^0}$ is specified by two ray parameters $\gamma^{(J)}$, chosen as two take-off angles, ϕ_0 and δ_0:

$$n_1^0 = \cos\phi_0 \cos\delta_0, \quad n_2^0 = \sin\phi_0 \cos\delta_0, \quad n_3^0 = \sin\delta_0. \tag{6}$$

Pšenčík & Farra (2005) have shown that accuracy of traveltime computations can be increased by calculating a second-order traveltime correction along the first-order ray Ω_0:

$$\Delta\tau = -\frac{1}{2}\int_{\Omega_0} c^{-2}(x_m, n_m)\frac{B_{13}^2(x_m, n_m) + B_{23}^2(x_m, n_m)}{V_P^2 - V_S^2}\, d\tau. \tag{7}$$

It can be easily evaluated by numerical quadratures along the FORT ray; c^{-2} can be evaluated as $c^{-2} = p_k p_k$. V_P and V_S are *P*- and *S*-wave velocities of a reference isotropic medium closely approximating the studied weakly anisotropic medium. The velocity V_P has nothing to do with the velocity α used for the definition of the WA parameters, see eq. (A1). Thus, the choice of V_P is completely independent of the choice of α. Optimal choice of V_P is $V_P^2 = (p_k p_k)^{-1}$, where p_k are the components of the slowness vectors obtained by integration of the FORT system (1). For the determination of V_S, we can use the relation $V_S^2 = V_P^2/3$. Thus, V_P and V_S may vary along the ray. The quantities B_{13} and B_{23} are elements of the matrix

$$B_{ij}(x_m, n_m) = \Gamma_{kl}(x_m, n_m) e_k^i e_l^j, \tag{8}$$

see Farra & Pšenčík (2003) and Pšenčík & Farra (2005). For elements B_{13} and B_{23} see Appendix A, eq. (A3). The symbols e_m^j denote components of three mutually perpendicular unit vectors $\mathbf{e^1}$, $\mathbf{e^2}$ and $\mathbf{e^3}$. The vector $\mathbf{e^3}$ is identical to $\mathbf{n}$, $\mathbf{e^3} = \mathbf{n}$. The matrix B_{mn}, as $G(x_m, p_m)$, is independent of the choice of the reference

velocity α. Moreover, the expression $B_{13}^2 + B_{23}^2$ is also independent of the choice of the vectors $\mathbf{e^1}$ and $\mathbf{e^2}$ in the plane perpendicular to $\mathbf{e^3}$.

3 FIRST-ORDER *P*-WAVE RAY THEORY GREEN'S FUNCTION

Basic step in the computation of ray synthetic seismograms is the computation of the ray theory Green's function. The ray theory Green's function $G_{in}(R, t, S, t_0)$ represents the ith component of the displacement vector at a receiver R and time t due to a single-force point source acting at S and oriented along the nth Cartesian coordinate axis, with the time dependence $\delta(t - t_0)$. The ray theory Green's function belongs to a selected elementary wave, in our case, to the P wave. The Fourier transform of the ray theory Green's function $G_{in}(R, t, S, t_0)$ with respect to $t - t_0$ reads (see e.g. Červený 2001; Červený *et al.* 2007):

$$G_{in}(R, S, \omega) = \frac{g_n(S) g_i(R) \exp[\mathrm{i} T^G(R, S) + \mathrm{i}\omega\tau(R, S)]}{4\pi[\rho(S)\rho(R)c(S)c(R)]^{1/2}\mathcal{L}(R, S)}. \tag{9}$$

The first-order ray theory Green's function is described by formally the same expression as in eq. (9). The first-order ray theory Green's function is, however, calculated along first-order rays and some of quantities, on which it depends, are of the first order. In this way, in eq. (9), g_i are components of the first-order polarization vectors, symbols c denote the first-order phase velocities. The symbol $\tau(R, S)$ denotes the first-order traveltime from S to R calculated along a ray determined by solving the FORT system (1). The first-order traveltime can be substituted by more accurate second-order traveltime including the traveltime correction (7). The symbol $T^G(R, S)$ is the complete phase shift due to caustics along the ray from S to R and ρ denotes the density.

The first-order or second-order traveltime $\tau(R, S)$, the first-order slowness vector components, p_i, and phase velocities c can be obtained as a solution of the FORT equations (1). The first-order P-wave polarization vector components, g_i, can be determined from the formula (see Farra & Pšenčík 2003):

$$g_i = n_i + \frac{B_{13}(x_m, n_m)e_i^1 + B_{23}(x_m, n_m)e_i^2}{V_P^2 - V_S^2}. \tag{10}$$

All the quantities appearing in eq. (10) have been described after eq. (7) for the second-order traveltime correction. Note that the components g_i constitute a unit vector only approximately.

The symbol $\mathcal{L}(R, S)$ denotes the first-order relative geometrical spreading (basic quantity affecting ray amplitudes)

$$\mathcal{L}(R, S) = \left|\mathbf{X}^{(1)} \times \mathbf{X}^{(2)}\right|^{1/2} \tag{11}$$

along the ray from S to R. Eq. (11) holds for the vectors $\mathbf{X}^{(I)}$ and other important vectors $\mathbf{Y}^{(I)}$, defined below, determined from the first-order dynamic ray tracing system with especially chosen initial conditions, given below, see also Pšenčík & Teles (1996). For the sake of brevity, we call $\mathcal{L}(R, S)$ the geometrical spreading in the following. If we denote the ray parameters specifying the FORT ray (i.e. the initial angles, ϕ_0 and δ_0) by $\gamma^{(I)}$, the components of the vectors $\mathbf{X}^{(I)}$ and $\mathbf{Y}^{(I)}$ can be expressed as

$$X_i^{(I)} = \left[\frac{\partial x_i}{\partial \gamma^{(I)}}\right]_{\tau=\mathrm{const}}, \quad Y_i^{(I)} = \left[\frac{\partial p_i}{\partial \gamma^{(I)}}\right]_{\tau=\mathrm{const}}. \tag{12}$$

The quantities $X_i^{(I)}$ and $Y_i^{(I)}$ describe variations along the wave front of the coordinates x_i and of the components p_i of the slowness vector due to the variations of the parameters $\gamma^{(I)}$. The values of $X_i^{(I)}$ and $Y_i^{(I)}$ can be found from a system of linear differential equations obtained by the differentiation of the FORT equations (1) with respect to $\gamma^{(I)}$:

$$\frac{dX_i^{(I)}}{d\tau} = \frac{1}{2}\left[\frac{\partial^2 G(x_m, p_m)}{\partial p_i \partial x_j} X_j^{(I)} + \frac{\partial^2 G(x_m, p_m)}{\partial p_i \partial p_j} Y_j^{(I)}\right],$$
$$\frac{dY_i^{(I)}}{d\tau} = -\frac{1}{2}\left[\frac{\partial^2 G(x_m, p_m)}{\partial x_i \partial x_j} X_j^{(I)} + \frac{\partial^2 G(x_m, p_m)}{\partial x_i \partial p_j} Y_j^{(I)}\right]. \tag{13}$$

The system of equations (13) is the FODRT system. Explicit expressions for the second derivatives of the P-wave first-order eigenvalue $G(x_m, p_m)$ of the Christoffel matrix are given in Appendix B. For vanishing anisotropy, equations (13) reduce to the corresponding exact equations for isotropic media. We obtain the quantities $X_i^{(J)}$ required for the calculation of the relative geometrical spreading, see eq. (11), by specifying the initial conditions for the FODRT equations (13) in the following way:

$$X_i^{(J)} = 0, \quad Y_i^{(J)} = c_0^{-1}\left(Z_{iJ} - p_i^0 v_{0k} Z_{kJ}\right), \tag{14}$$

where

$$Z_{11} = -\sin\phi_0 \cos\delta_0, \quad Z_{21} = \cos\phi_0 \cos\delta_0, \quad Z_{31} = 0,$$
$$Z_{12} = -\cos\phi_0 \sin\delta_0, \quad Z_{22} = -\sin\phi_0 \sin\delta_0, \quad Z_{32} = \cos\delta_0, \tag{15}$$

see Pšenčík & Teles (1996). In eq. (14), c_0 denotes, as before, the first-order phase velocity at the initial point S, v_{0i} denotes components of the first-order ray velocity vector, $v_i = dx_i/d\tau$, at the same point. The symbols ϕ_0 and δ_0 in eq. (15) denote again the take-off angles introduced in eq. (6).

The solution of FODRT equations (13) provides a tool for the determination of the complete phase shift due to caustics $T^G(R, S)$, see, for example, Červený *et al.* (2007). Moreover, the solution of FODRT equations (13) can be also effectively used for the two-point ray tracing based on shooting. The quantities $X_i^{(J)}$ are then used for estimation of the ray parameters $\gamma^{(J)}$ (take-off angles ϕ_0 and δ_0) from the distance between termination points of rays shot at a receiver surface (surface containing receivers) and the receiver, at which the two-point ray should terminate.

4 NUMERICAL EXAMPLES

In the following, we show examples illustrating the accuracy of the proposed method. We consider the same VSP configuration and models as Pšenčík & Farra (2005), who studied only accuracy of the computed first- and second-order traveltimes. Here, we study accuracy of the geometrical spreading and of the first-order ray synthetic seismograms. The VSP configuration used in the tests is shown in Fig. 1.

The source and the borehole are situated in a vertical plane (x, z). The borehole lies along the z axis, the vertical single-force source is located on the surface at $z = 0$ km, at a distance of 1 km from the borehole. The source time function is a windowed symmetric Gabor wavelet $\exp[-(2\pi f/\gamma)^2 t^2] \cos(2\pi f t)$ with the dominant frequency $f = 25$ Hz and $\gamma = 4.44$. There are 24 receivers in the borehole, distributed with a uniform step size of 0.04 km, with receiver depths ranging from 0.04 to 0.96 km. The three-component receivers record the vertical (positive downwards), transverse and radial (along the line source—top of the borehole; positive away from the source) components of the wave field. The recording system is right-handed. All calculated seismograms are shown with no

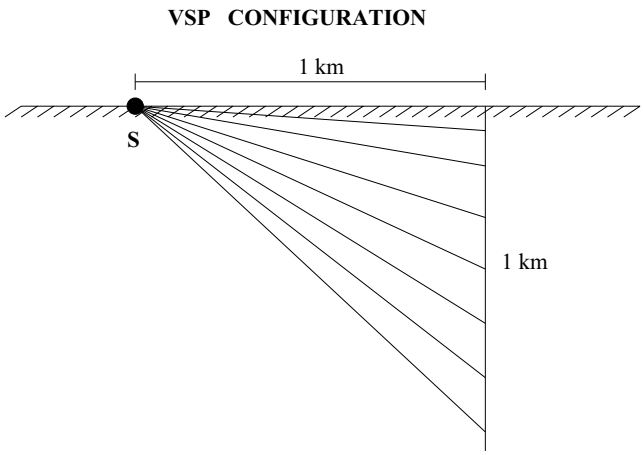

Figure 1. Schematic configuration of experiments.

differential scaling between components and traces, so true relative amplitudes can be seen. We consider two types of models: one transversely isotropic (models 'TI') and one orthorhombic (models 'ORTHO'). If we use common measure of *P*-wave anisotropy (maximum of $|\epsilon| \times 100$ per cent, where ϵ stands for ϵ_x, ϵ_y or ϵ_z), the anisotropy of the *P* wave in the models 'TI' is about 8 per cent and in the models 'ORTHO' about 20 per cent. As in Pšenčík & Farra (2005), we consider, for simplicity, only vertical variation of parameters of the medium. The procedure can, however, be applied to arbitrary laterally varying weakly anisotropic structures. The stiffness matrices are specified at the top of the model, at $z = 0$ km, and at a depth of $z = 3$ km. The values of the elements of the stiffness matrices are interpolated linearly between the two levels.

In the following, we measure the accuracy of the FORT and FODRT in the two types of models by plotting the relative differences of the geometrical spreading

$$\frac{\mathcal{L}_{\mathrm{FORT}} - \mathcal{L}_{\mathrm{EXACT}}}{\mathcal{L}_{\mathrm{EXACT}}} \times 100 \text{ per cent}. \tag{16}$$

The geometrical spreading values $\mathcal{L}_{\mathrm{FORT}}$ are obtained by the approach described in the preceding sections, that is, by solving the FODRT equations (13). The geometrical spreading values $\mathcal{L}_{\mathrm{EXACT}}$ are computed by a standard ray tracer for anisotropic media—a modified version of the program package ANRAY (Gajewski & Pšenčík 1990).

In addition to the plots of relative differences of the geometrical spreading, we also present comparison of resulting ray synthetic seismograms. All seismograms are shifted by 0.03 s in order to shift the traveltimes from the maxima of the Gabor wavelet to, approximately, their onsets. FORT seismograms are in red, exact ray synthetic seismograms are in black. First-order traveltimes are used in the seismograms for the 'TI' models, second-order traveltime correction (7) is used in the seismograms for the 'ORTHO' models. In (7), we use $V_S^2 = V_P^2/3$ and $V_P^2 = (p_k p_k)^{-1}$, where p_k are the components of the first-order slowness vectors obtained during the integration of the FORT equations (1). The values of V_P and V_S determined in the above way yield the best results. Dependence of the results on the V_P/V_S ratio is negligible.

4.1 'TI' models

The density-normalized stiffness matrices of TI models with elements, measured in $(\mathrm{km\ s^{-1}})^2$, are:

$$\begin{pmatrix} 15.71 & 5.05 & 4.46 & 0. & 0. & 0. \\ & 15.71 & 4.46 & 0. & 0. & 0. \\ & & 13.39 & 0. & 0. & 0. \\ & & & 4.98 & 0. & 0. \\ & & & & 4.98 & 0. \\ & & & & & 5.33 \end{pmatrix}$$

at $z = 0$ km, and

$$\begin{pmatrix} 35.35 & 11.36 & 10.04 & 0. & 0. & 0. \\ & 35.35 & 10.04 & 0. & 0. & 0. \\ & & 30.13 & 0. & 0. & 0. \\ & & & 11.21 & 0. & 0. \\ & & & & 11.21 & 0. \\ & & & & & 11.99 \end{pmatrix} \tag{17}$$

at $z = 3$ km. The stiffness matrices in eq. (17) are based on the Voigt notation. The variations of the *P*-wave phase velocities in a vertical plane from horizontal (0°) to vertical (90°) direction of the normal to the wave front are shown in Fig. 2, for $z = 0$ and 3 km, respectively. Numerical experiments were performed for three specific models: 'HTI', 'ISO' and 'HTI-ROT', described below.

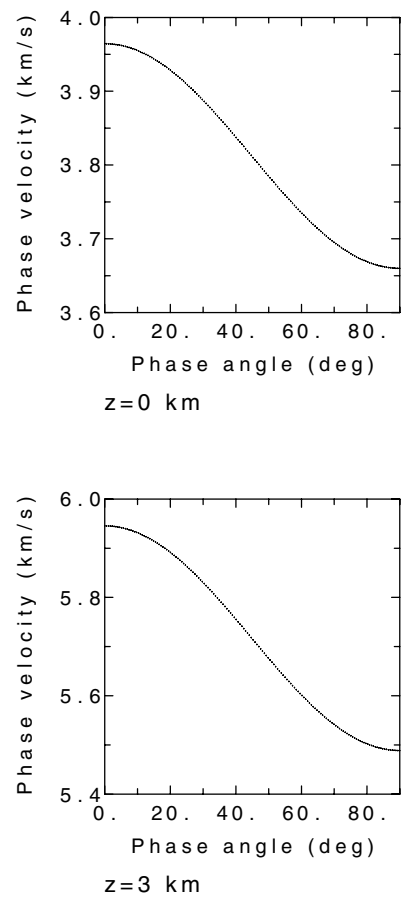

Figure 2. *P*-wave phase-velocity variations corresponding to stiffness matrices for the TI model specified in eq. (17) from horizontal (0°) to vertical (90°) direction of the normal to the wave front.

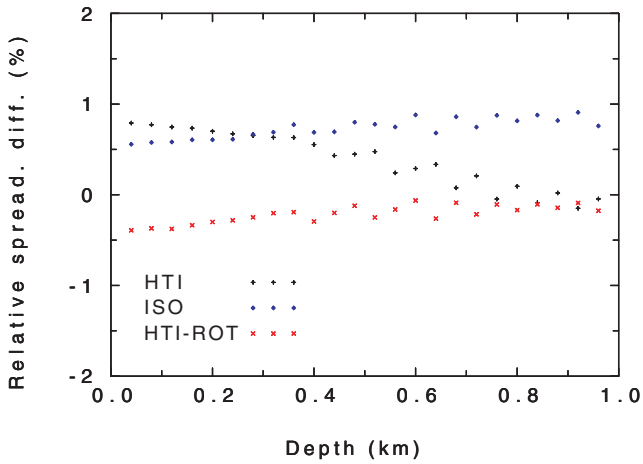

Figure 3. Relative geometrical-spreading differences, see eq. (16), for the models 'HTI' (black), 'ISO' (blue) and 'HTI–ROT' (red).

Fig. 3 shows the relative differences of the geometrical spreading, see eq. (16), for the models 'HTI' (black), 'ISO' (blue) and 'HTI-ROT' (red), respectively. The model 'HTI' is obtained from the model specified in eq. (17) by rotating the axes of symmetry at the top and the bottom of the model so that they are parallel to the x axis, that is, to the line connecting the source and the top of the borehole. In contrast to behaviour of the traveltime, see fig. 3 of Pšenčík & Farra (2005), the first-order geometrical spreading is less accurate for shallow receivers, the relative error reaching nearly 1 per cent. With increasing depth of receivers the error decreases to effectively 0 per cent at $z = 1$ km. The model 'ISO' is obtained from the model given by eq. (17) by orienting the axes of symmetry at the planes $z =$ 0 and 3 km perpendicularly to the vertical (x, z) plane containing the source and the borehole. In this case the relative error, see eq. (16), slightly increases with depth, from about 0.5 per cent to nearly 1 per cent. In both mentioned cases, the first-order geometrical spreading $\mathcal{L}_{\mathrm{FORT}}$ slightly exceeds the value of $\mathcal{L}_{\mathrm{EXACT}}$. This is different in the 'HTI-ROT' model. In this model, the axis of symmetry deviates by 45° from the x axis in the horizontal plane $z = 0$ km. At $z = 3$ km, it is oriented along the x axis. In between, as depth varies, the axis of symmetry is smoothly rotated, remaining horizontal. The relative errors are least in this case, they vary from about -0.4 per cent at z $= 0$ km to nearly 0 per cent at $z = 1$ km.

In Fig. 4, we show comparison of exact (black) and first-order (red) ray synthetic seismograms for the model 'HTI'. Only radial and vertical components are shown since the transverse component is identically zero (the plane (x, z) coincides with the plane of symmetry and the source is a vertical force). First-order traveltimes obtained by integration of the FORT equations (1) are used. Since maximum relative traveltime errors are less than 0.15 per cent and maximum relative geometrical spreading errors are less than 1 per cent in this case, see fig. 3 of Pšenčík & Farra (2005) and Fig. 3 here, respectively, the fit of the seismograms is perfect.

4.2 'ORTHO' models

As a next model, we consider the model of Schoenberg & Helbig (1997). It has anisotropy substantially larger than the TI models previously considered. The anisotropy is about 20 per cent. The density-normalized stiffness matrices of the 'ORTHO' models with

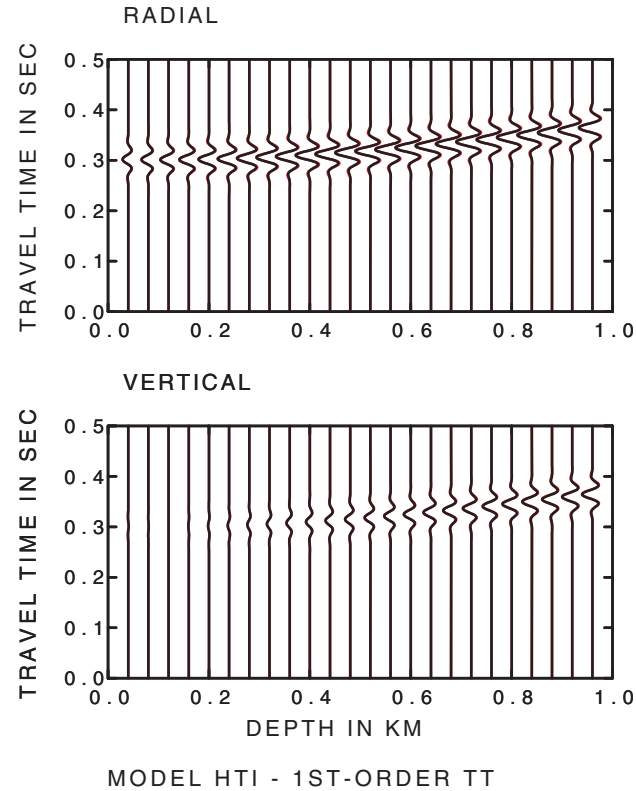

Figure 4. Comparison of the first-order (red) and exact (black) ray synthetic seismograms for the vertical single-force source in the 'HTI' model. First-order traveltimes obtained by solving eq. (1) are used.

elements measured in $(\mathrm{km\,s^{-1}})^2$, are at the top, $z = 0$ km:

$$\begin{pmatrix} 9.00 & 3.60 & 2.25 & 0. & 0. & 0. \\ & 9.84 & 2.40 & 0. & 0. & 0. \\ & & 5.94 & 0. & 0. & 0. \\ & & & 2.00 & 0. & 0. \\ & & & & 1.60 & 0. \\ & & & & & 2.18 \end{pmatrix}$$

and at the bottom, $z = 3$ km:

$$\begin{pmatrix} 19.80 & 7.92 & 4.95 & 0. & 0. & 0. \\ & 21.65 & 5.28 & 0. & 0. & 0. \\ & & 13.07 & 0. & 0. & 0. \\ & & & 4.40 & 0. & 0. \\ & & & & 3.52 & 0. \\ & & & & & 4.80 \end{pmatrix}. \qquad (18)$$

Variations of the P-wave phase velocities in the vertical (x, z) plane (left-hand column) and the vertical (y, z) plane (right-hand column) are shown in Fig. 5 from horizontal (0°) to vertical (90°) direction of the normal to the wave front, for the top and the bottom of the model. Numerical experiments were performed for two specific models: ORT and ORT–ROT, described below.

Fig. 6 shows relative differences, see eq. (16), of the geometrical spreading (black) and of vertical component of the polarization vector at the source (red) for the model 'ORT', that is, for the (x, z) plane of the model specified in eq. (18). The mentioned two

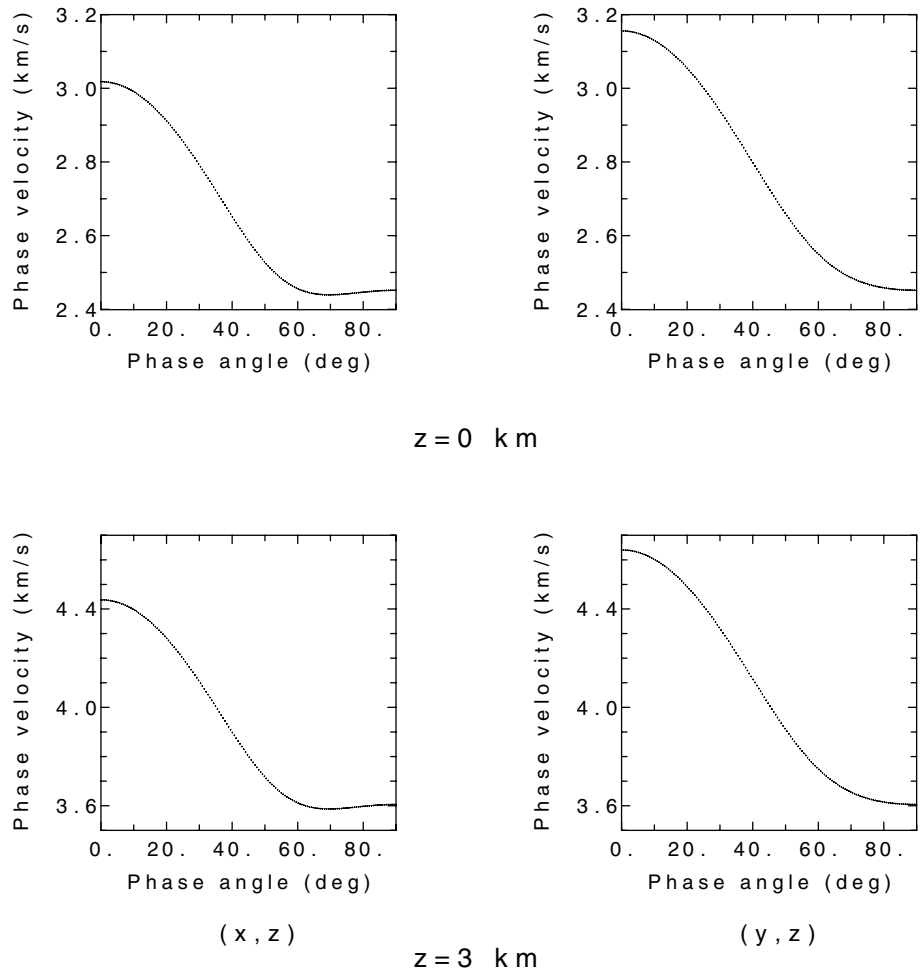

Figure 5. *P*-wave phase-velocity variations corresponding to stiffness matrices for the ORTHO model specified in eq. (18) from horizontal (0°) to vertical (90°) direction of the normal to the wave front. The upper plots correspond to $z = 0$ km, the lower plots to $z = 3$ km, the left-hand column to the (x, z) plane, the right-hand column to the (y, z) plane.

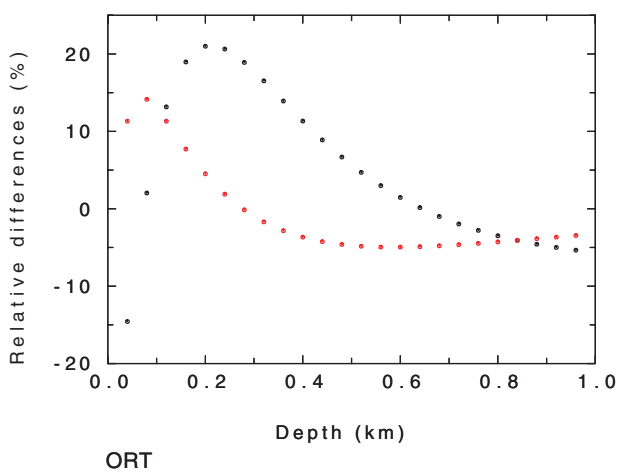

Figure 6. Relative differences, see eq. (16), of the geometrical spreading (black), see eq. (11), and of vertical components of the polarization vectors at the source (red), see eq. (10), for the model 'ORT'.

quantities show most significant differences and have most pronounced effects on accuracy of the first-order synthetic seismograms shown in Fig. 7. In comparison with these two quantities, differences of horizontal components of the polarization vectors at receivers as well as of phase velocities at the source and at receivers are negligible. The differences of vertical components of the polarization vectors at receivers, which are comparable with those of vertical components of the polarization vectors at the source, are not shown. The differences in Fig. 6 have an oscillating character. Due to the stronger anisotropy the maximum difference of the geometrical spreading reaches nearly −20 per cent around $z = 0$ km, and slightly exceeds 20 per cent for depths around 0.2 km. The maximum difference of vertical components of the polarization vector at the source reaches 15 per cent for depths around 0.1 km. Note that the error of the first-order traveltime was also relatively large, more than 1.5 per cent for this model. As explained in Pšenčík & Farra (2005), the differences are caused by errors of the first-order approximation $G^{(1)}$ (specifically of the curvature of the surface $G^{(1)} = 1$) in the direction from the source towards the shallow receivers. With increasing depth, the differences decrease and become slightly negative for deepest receivers.

Fig. 7 shows a comparison of the ray synthetic seismograms generated by the vertical force in the 'ORT' model. Exact seismograms and their first-order approximations are shown in black and red, respectively. Only radial and vertical components are shown since the transverse component is again identically zero (the plane (x, z) coincides with the plane of symmetry and the source is a vertical force). This time, second-order traveltime correction (7) is used because of

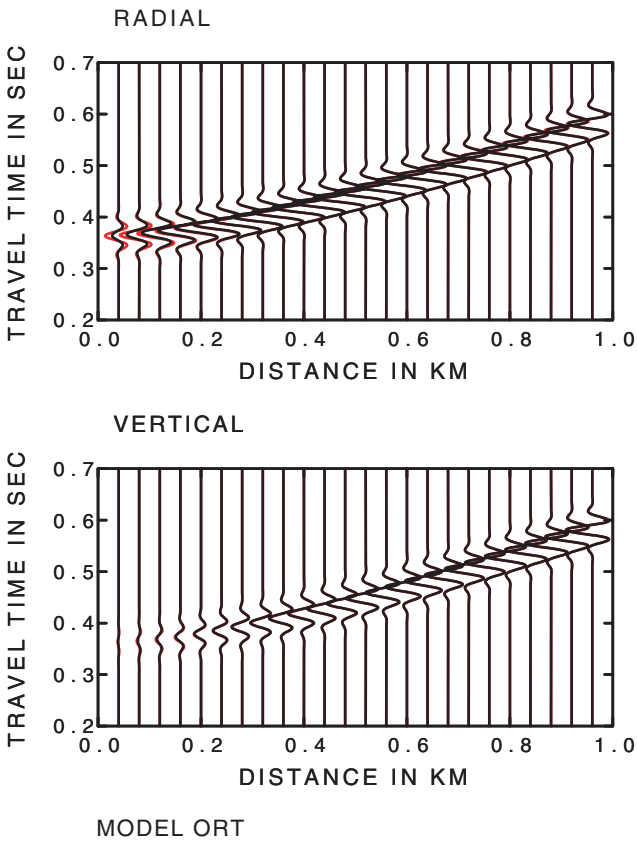

Figure 7. Comparison of the first-order (red) and exact (black) ray synthetic seismograms for the vertical single-force source in the 'ORT' model. Second-order traveltime correction (7) used.

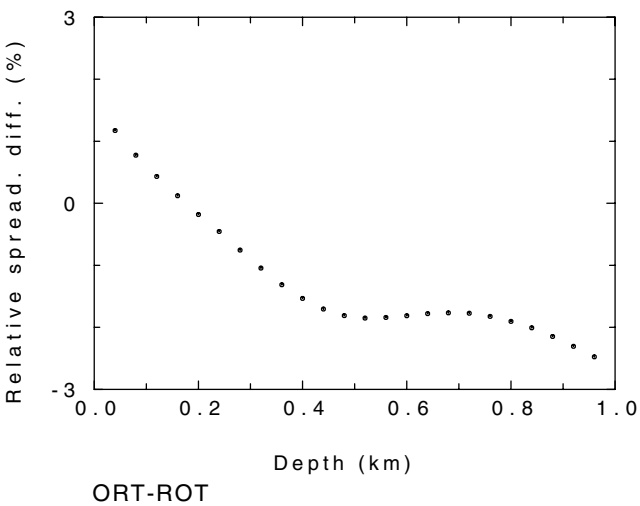

Figure 8. Relative geometrical-spreading differences, see eq. (16), for the model 'ORT–ROT'.

non-negligible first-order traveltime errors, see fig. 7 of Pšenčík & Farra (2005). In contrast to Fig. 4, we can see some differences in Fig. 7. They concentrate at depths between 0 and 0.2 km on radial component (on vertical component they are suppressed by small amplitudes). The differences on the radial component are a result of combined effects of the errors of the approximation of the geometrical spreading and of vertical component of the polarization

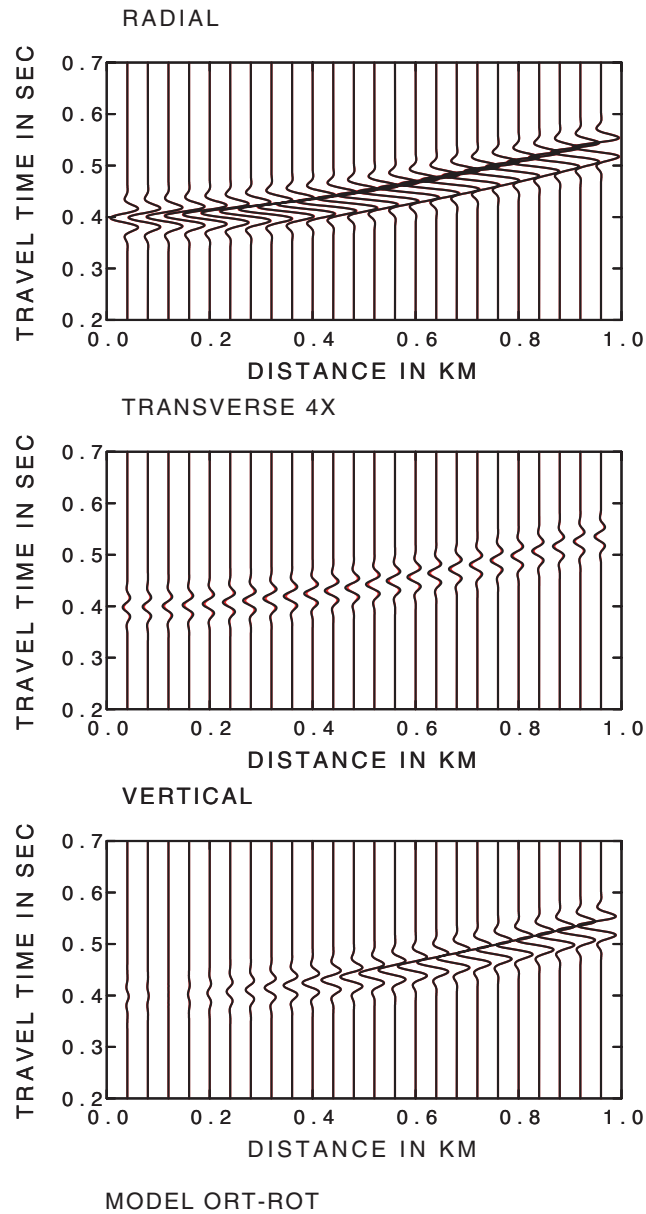

Figure 9. Comparison of the first-order (red) and exact (black) ray synthetic seismograms for the vertical single-force source in the 'ORT-ROT' model. Second-order traveltime correction (7) used.

vector at the source, see Fig. 6. At the shallowest receiver, errors of both quantities lead to an increase of amplitudes of the first-order seismograms. At the second receiver, the increase of amplitudes is caused, practically solely, by the error of the first-order polarization vector, see Fig. 6. At deeper receivers, errors of both quantities approximately compensate each other.

As Pšenčík & Farra (2005), we also consider a model 'ORT–ROT', which results from a different rotation of matrices in eq. (18). The upper matrix of the model in eq. (18) is first rotated by 45^o around z axis, and then the z axis is rotated by 45^o around the new y axis. The matrix corresponding to a depth of $z = 3$ km is kept unrotated. Similarly as the relative traveltime differences, see fig. 8 of Pšenčík & Farra (2005), also the relative geometrical spreading differences, see eq. (16), are significantly smaller in this case than for the 'ORT' model, see Fig. 8. They are about 1 per cent for

the shallowest receivers, decrease to 0 per cent and then decrease to nearly −3 per cent. Because of the small deviations, the comparison of ray synthetic seismograms (black) with their first-order approximation (red) in Fig. 9 gives a nearly perfect fit. In the first-order seismograms in Fig. 9, the second-order traveltime correction (7) is used.

5 CONCLUSIONS

We have extended the applicability of the FORT approach for *P* waves propagating in smooth, laterally inhomogeneous, weakly anisotropic media of arbitrary symmetry, proposed by Pšenčík & Farra (2005), to the evaluation of the first-order ray amplitudes and, in this way, also the first-order ray synthetic seismograms. As shown in this paper, the relative errors of amplitudes (specifically of the geometrical spreading) are generally larger than the relative traveltime errors. Nevertheless, in configurations as those considered in this paper, FORT and FODRT provide results with small deviations from exact ones, but with several important advantages:

(1) FORT and FODRT equations are expressed in terms of the WA parameters, which represent a more natural description of a weakly anisotropic medium than standard elastic moduli.

(2) FORT and FODRT equations have a considerably simpler structure than the exact ones, which leads to a significant reduction of the number of algebraic operations involved.

(3) In the most general case, they depend only on the 15 *P*-wave WA parameters.

(4) As the FORT and FODRT equations allow *P* waves to be treated separately from *S* waves, as in isotropic media, they can easily be used as substitutes for traditional 'isotropic' ray and dynamic ray tracers in many routine applications such as prestack Kirchhoff depth migration.

(5) The FORT and FODRT equations are applicable to inhomogeneous isotropic as well as anisotropic media. In isotropic media they yield exact rays and exact dynamic ray tracing results, in anisotropic media their first-order approximations.

As in the case of the FORT equations, the FODRT equations seem to show only very weak dependence of the accuracy of their solution on the strength of the inhomogeneity of the medium. The accuracy depends more on the strength of considered anisotropy, not so much on its type.

In this paper, the dynamic ray tracing was used only for the computation of the geometrical spreading and in the two-point ray tracing procedure. Like the exact dynamic ray tracing, also FODRT has many additional important applications, see Červený (2001) for the extensive list of these applications. Use of the propagator technique, see, for example, Červený (2001; section 4.3), to solve eq. (13) is straightforward.

Generalization of the described procedure for layered, laterally varying, weakly anisotropic media is under way. Extension to inhomogeneous, weakly anisotropic media with weak attenuation is also considered. Further plans include studies of *S* waves in inhomogeneous weakly anisotropic media (Farra 2005). In this respect, one option is use of the quasi-isotropic approximation (Pšenčík 1998) for *S* waves. The FORT and FODRT formulae for media of higher-symmetry anisotropy will certainly find applications in procedures for ray tracing and dynamic ray tracing in structures with continuously varying orientation of symmetry axes or planes (Iversen & Pšenčík 2007).

ACKNOWLEDGMENTS

The authors are grateful to Sláva Červený for his constructive comments. Comments of two anonymous reviewers helped to improve the MS considerably. Substantial part of this work was done during IP's stay at the IPG Paris on the invitation of the IPGP. We are grateful to consortium project 'Seismic waves in complex 3-D structures' (SW3D), Research Project 205/05/2182 of the Grant Agency of the Czech Republic and Research Project A3012309 of the Grant Agency of the Academy of Sciences of the Czech Republic for support. Part of this work was also done during the European Union Transfer of Knowledge project IMAGES (MTKI-CT-2004-517242).

REFERENCES

Červený, V., 2001. *Seismic Ray Theory*, Cambridge Univ. Press, Cambridge.

Červený, V., Klimeš, L. & Pšenčík, I., 2007. Seismic Ray method: recent developments, in *Advances in Geophysics*, Vol. 48: 'Advances in Wave Propagation in Heterogeneous Earth', pp. 1–126, eds Wu, R.-S. & Maupin, V., series editor Dmowska, R., Elsevier Academic Press, San Diego.

Farra, V., 2005. First-order ray tracing for *qS* waves in inhomogeneous weakly anisotropic media, *Geophys. J. Int.,* **161,** 309–324.

Farra, V. & Pšenčík, I., 2003. Properties of the zero-, first- and higher-order approximations of attributes of elastic waves in weakly anisotropic media, *J. acoust. Soc. Am.,* **114,** 1366–1378.

Gajewski, D. & Pšenčík, I., 1990. Vertical seismic profile synthetics by dynamic ray tracing in laterally varying layered anisotropic structures, *J. geophys. Res.,* **95,** 11 301–11 315.

Iversen, E. & Pšenčík, I., 2007. Ray tracing for continuously rotated local coordinates belonging to a specified anisotropy. *Stud. Geophys. Geod.,* **51,** 37–58.

Pšenčík, I., 1998. Green's functions for inhomogeneous weakly anisotropic media, *Geophys. J. Int.,* **135,** 279–288.

Pšenčík, I. & Farra, V., 2005. First-order ray tracing for qP waves in inhomogeneous weakly anisotropic media, *Geophysics,* **70,** D65–D75.

Pšenčík, I. & Gajewski, D., 1998. Polarization, phase velocity and NMO velocity of *qP* waves in arbitrary weakly anisotropic media, *Geophysics,* **63,** 1754–1766.

Pšenčík, I. & Teles, T.N., 1996. Point source radiation in inhomogeneous anisotropic structures, *Pageoph,* **148,** 591–623.

Schoenberg, M. & Helbig, K., 1997. Orthorhombic media: Modeling elastic wave behavior in a vertically fractured earth, *Geophysics,* **62,** 1954–1974.

Thomsen, L., 1986. Weak elastic anisotropy, *Geophysics,* **51,** 1954–1966.

APPENDIX A: *P*-WAVE WA PARAMETERS

If we denote by α the velocity of a reference isotropic medium, we can introduce 15 *P*-wave WA parameters in the following way:

$$\epsilon_x = \frac{A_{11}-\alpha^2}{2\alpha^2}, \quad \epsilon_y = \frac{A_{22}-\alpha^2}{2\alpha^2}, \quad \epsilon_z = \frac{A_{33}-\alpha^2}{2\alpha^2},$$
$$\delta_x = \frac{A_{13}+2A_{55}-\alpha^2}{\alpha^2}, \quad \delta_y = \frac{A_{23}+2A_{44}-\alpha^2}{\alpha^2}, \quad \delta_z = \frac{A_{12}+2A_{66}-\alpha^2}{\alpha^2},$$
$$\chi_x = \frac{A_{14}+2A_{56}}{\alpha^2}, \quad \chi_y = \frac{A_{25}+2A_{46}}{\alpha^2}, \quad \chi_z = \frac{A_{36}+2A_{45}}{\alpha^2},$$
$$\epsilon_{15} = \frac{A_{15}}{\alpha^2}, \quad \epsilon_{16} = \frac{A_{16}}{\alpha^2}, \quad \epsilon_{24} = \frac{A_{24}}{\alpha^2}, \quad \epsilon_{26} = \frac{A_{26}}{\alpha^2}, \quad \epsilon_{34} = \frac{A_{34}}{\alpha^2} \text{ and } \epsilon_{35} = \frac{A_{35}}{\alpha^2}. \tag{A1}$$

Here $A_{\alpha\beta}$ are the density-normalized elastic moduli in the Voigt notation.

The following variables have also been used:

$$\eta_x = \delta_y - \epsilon_y - \epsilon_z, \quad \eta_y = \delta_x - \epsilon_x - \epsilon_z, \quad \eta_z = \delta_z - \epsilon_x - \epsilon_y. \tag{A2}$$

The elements B_{13} and B_{23} of the matrix B_{mn}, see eq. (8), can be expressed explicitly in the following way:

$$\begin{aligned}
B_{13} = {} & \alpha^2 D^{-1}\left\{n_3^4(\epsilon_{34}n_2+\epsilon_{35}n_1)+n_3^3\left[\eta_y n_1^2+\eta_x n_2^2+2\chi_z n_1 n_2\right]\right. \\
& +n_3^2\left[(4\chi_x-3\epsilon_{34})n_1^2 n_2+(4\chi_y-3\epsilon_{35})n_1 n_2^2+(4\epsilon_{15}-3\epsilon_{35})n_1^3+(4\epsilon_{24}-3\epsilon_{34})n_2^3\right] \\
& +n_3\left[(2\eta_z-\eta_x-\eta_y)n_1^2 n_2^2+2(2\epsilon_{16}-\chi_z)n_1^3 n_2+2(2\epsilon_{26}-\chi_z)n_1 n_2^3\right. \\
& \left.\left.-\eta_y n_1^4-\eta_x n_2^4+(\epsilon_x-\epsilon_z)n_1^2+(\epsilon_y-\epsilon_z)n_2^2\right]-\chi_x n_1^2 n_2-\chi_y n_1 n_2^2-\epsilon_{15}n_1^3-\epsilon_{24}n_2^3\right\}, \\
B_{23} = {} & \alpha^2 D^{-1}\left\{n_3^3(\epsilon_{34}n_1-\epsilon_{35}n_2)+n_3^2\left[(\eta_x-\eta_y)n_1 n_2+\chi_z n_1^2-\chi_z n_2^2\right]\right. \\
& +n_3\left[(2\chi_y-3\epsilon_{15})n_1^2 n_2-(2\chi_x-3\epsilon_{24})n_1 n_2^2+\chi_x n_1^3-\chi_y n_2^3\right] \\
& \left.+\eta_z n_1^3 n_2-\eta_z n_1 n_2^3+3(\epsilon_{26}-\epsilon_{16})n_1^2 n_2^2+\epsilon_{16}n_1^4-\epsilon_{26}n_2^4+(\epsilon_y-\epsilon_x)n_1 n_2\right\}.
\end{aligned} \tag{A3}$$

The expressions in eq. (A3) correspond to the following choice of vectors $\mathbf{e}^i$ in eq. (8):

$$\mathbf{e}^1 \equiv D^{-1}\left(n_1 n_3, n_2 n_3, n_3^2-1\right), \quad \mathbf{e}^2 \equiv D^{-1}(-n_2, n_1, 0), \quad \mathbf{e}^3 = \mathbf{n} \equiv (n_1, n_2, n_3), \tag{A4}$$

where

$$D = \left(n_1^2+n_2^2\right)^{1/2}, \qquad n_1^2+n_2^2+n_3^2 = 1. \tag{A5}$$

The symbols n_i denote components of the unit normal to the wave front.

APPENDIX B: EXPRESSIONS FOR THE FIRST AND SECOND DERIVATIVES OF THE FIRST-ORDER *P*-WAVE EIGENVALUE *G* FOR AN ANISOTROPIC MEDIUM OF ARBITRARY SYMMETRY

The first derivatives of the first-order *P*-wave eigenvalue in eq. (4) appearing on the RHS of FORT equations (1) depend on x_m and p_m. They have the following explicit form:

$$\begin{aligned}
\frac{\partial G}{\partial p_1} &= 2\alpha^2\left\{p_1+2\epsilon_x p_1+2c^4\left[A p_{23}p_1+B\left(p_{23}-p_1^2\right)+C\left(3p_{23}+p_1^2\right)p_1^2-D p_1 p_2 p_3\right]\right\}, \\
\frac{\partial G}{\partial p_2} &= 2\alpha^2\left\{p_2+2\epsilon_y p_2+2c^4\left[E p_{13}p_2+F\left(p_{13}-p_2^2\right)+G\left(3p_{13}+p_2^2\right)p_2^2-H p_1 p_2 p_3\right]\right\}, \\
\frac{\partial G}{\partial p_3} &= 2\alpha^2\left\{p_3+2\epsilon_z p_3+2c^4\left[P p_{12}p_3+Q\left(p_{12}-p_3^2\right)+R\left(3p_{12}+p_3^2\right)p_3^2-S p_1 p_2 p_3\right]\right\}, \\
\frac{\partial G}{\partial x_i} &= 2\alpha^2\left\{T_{,i}+c^2\left[2R_{,i}p_3^3+P_{,i}p_3^2+2Q_{,i}p_3+S_{,i}p_1p_2\right]\right\}.
\end{aligned} \tag{B1}$$

The second derivatives of the first-order *P*-wave eigenvalue in eq. (4) appearing on the RHS of FODRT equations (13) depend on x_m and p_m too. They have the following explicit form:

$$\begin{aligned}
\frac{\partial^2 G}{\partial p_1^2} &= 2\alpha^2\left\{1+2\epsilon_x+2c^6\left[(A p_{23}-D p_2 p_3)(p_{23}-3p_1^2)+2p_1(C p_{23}-B)\left(3p_{23}-p_1^2\right)\right]\right\}, \\
\frac{\partial^2 G}{\partial p_1 \partial p_2} &= 4\alpha^2\left\{c^4\left[2(\chi_x p_3+\eta_z p_2)p_1 p_{23}+\left(\chi_z p_3^2+2\chi_y p_2 p_3+3\epsilon_{26}p_2^2\right)\left(p_{23}-p_1^2\right)\right.\right. \\
&\quad \left.+\epsilon_{16}\left(p_1^2+3p_{23}\right)p_1^2-(\eta_x p_3+4\epsilon_{24}p_2)p_1 p_2 p_3\right]-c^6\left[2A(p_{23}-p_1^2)p_1 p_2+2B\left(p_{23}-3p_1^2\right)p_2\right. \\
&\quad \left.\left.+2C\left(3p_{23}-p_1^2\right)p_1^2 p_2+D\left(p_{13}-3p_2^2\right)p_1 p_3\right]\right\},
\end{aligned}$$

$$
\begin{aligned}
\frac{\partial^2 G}{\partial p_1 \partial p_3} &= 4\alpha^2 \{ c^4 \left[2(\chi_x p_2 + \eta_y p_3) p_1 p_{23} + \left(\chi_y p_2^2 + 2\chi_z p_2 p_3 + 3\epsilon_{35} p_3^2 \right) \left(p_{23} - p_1^2 \right) \right. \\
&\quad \left. + \epsilon_{15} \left(p_1^2 + 3p_{23} \right) p_1^2 - (\eta_x p_2 + 4\epsilon_{34} p_3) p_1 p_2 p_3 \right] - c^6 \left[2A \left(p_{23} - p_1^2 \right) p_1 p_3 + 2B \left(p_{23} - 3p_1^2 \right) p_3 \right. \\
&\quad \left. + 2C \left(3p_{23} - p_1^2 \right) p_1^2 p_3 + D \left(p_{12} - 3p_3^2 \right) p_1 p_2 \right] \}, \\
\frac{\partial^2 G}{\partial p_2^2} &= 2\alpha^2 \{ 1 + 2\epsilon_y + 2c^6 \left[(E p_{13} - H p_1 p_3)\left(p_{13} - 3p_2^2 \right) + 2p_2 (G p_{13} - F)(3p_{13} - p_2^2) \right] \}, \\
\frac{\partial^2 G}{\partial p_2 \partial p_3} &= 4\alpha^2 \{ c^4 \left[2(\chi_y p_1 + \eta_x p_3) p_2 p_{13} + \left(\chi_x p_1^2 + 2\chi_z p_1 p_3 + 3\epsilon_{34} p_3^2 \right)\left(p_{13} - p_2^2 \right) \right. \\
&\quad \left. + \epsilon_{24}\left(p_2^2 + 3p_{13} \right) p_2^2 - (\eta_y p_1 + 4\epsilon_{35} p_3) p_1 p_2 p_3 \right] - c^6 \left[2E\left(p_{13} - p_2^2 \right) p_2 p_3 + 2F\left(p_{13} - 3p_2^2 \right) p_3 \right. \\
&\quad \left. + 2G\left(3p_{13} - p_2^2 \right) p_2^2 p_3 + H\left(p_{12} - 3p_3^2 \right) p_1 p_2 \right] \}, \\
\frac{\partial^2 G}{\partial p_3^2} &= 2\alpha^2 \{ 1 + 2\epsilon_z + 2c^6 \left[(P p_{12} - S p_1 p_2)(p_{12} - 3p_3^2) + 2p_3 (R p_{12} - Q)\left(3p_{12} - p_3^2 \right) \right] \}, \\
\frac{\partial^2 G}{\partial x_i \partial p_1} &= 4\alpha^2 \{ \epsilon_{x,i} p_1 + c^4 \left[A_{,i} p_{23} p_1 + B_{,i}\left(p_{23} - p_1^2 \right) + C_{,i}\left(3p_{23} + p_1^2 \right) p_1^2 - D_{,i} p_1 p_2 p_3 \right] \}, \\
\frac{\partial^2 G}{\partial x_i \partial p_2} &= 4\alpha^2 \{ \epsilon_{y,i} p_2 + c^4 \left[E_{,i} p_{13} p_2 + F_{,i}\left(p_{13} - p_2^2 \right) + G_{,i}\left(3p_{13} + p_2^2 \right) p_2^2 - H_{,i} p_1 p_2 p_3 \right] \}, \\
\frac{\partial^2 G}{\partial x_i \partial p_3} &= 4\alpha^2 \{ \epsilon_{z,i} p_3 + c^4 \left[P_{,i} p_{12} p_3 + Q_{,i}\left(p_{12} - p_3^2 \right) + R_{,i}\left(3p_{12} + p_3^2 \right) p_3^2 - S_{,i} p_1 p_2 p_3 \right] \}, \\
\frac{\partial^2 G}{\partial x_i \partial x_j} &= 2\alpha^2 \{ T_{,ij} + c^2 \left[2R_{,ij} p_3^3 + P_{,ij} p_3^2 + 2Q_{,ij} p_3 + S_{,ij} p_1 p_2 \right] \}.
\end{aligned}
\tag{B2}
$$

In eqs (B1) and (B2),

$$
c^2 = (p_k p_k)^{-1}, \tag{B3}
$$

and the following notation is used:

$$
\begin{aligned}
p_{13} &= p_1^2 + p_3^2, \quad p_{23} = p_2^2 + p_3^2, \quad p_{12} = p_1^2 + p_2^2, \\
A &= \eta_y p_3^2 + 2\chi_x p_2 p_3 + \eta_z p_2^2, \quad B = \epsilon_{35} p_3^3 + \chi_z p_2 p_3^2 + \chi_y p_2^2 p_3 + \epsilon_{26} p_2^3, \\
C &= \epsilon_{15} p_3 + \epsilon_{16} p_2, \quad D = 2\epsilon_{34} p_3^2 + \eta_x p_2 p_3 + 2\epsilon_{24} p_2^2, \\
E &= \eta_x p_3^2 + 2\chi_y p_1 p_3 + \eta_z p_1^2, \quad F = \epsilon_{34} p_3^3 + \chi_z p_1 p_3^2 + \chi_x p_1^2 p_3 + \epsilon_{16} p_1^3, \\
G &= \epsilon_{24} p_3 + \epsilon_{26} p_1, \quad H = 2\epsilon_{35} p_3^2 + \eta_y p_1 p_3 + 2\epsilon_{15} p_1^2, \\
P &= \eta_y p_1^2 + 2\chi_z p_1 p_2 + \eta_x p_2^2, \quad Q = \epsilon_{15} p_1^3 + \chi_x p_1^2 p_2 + \chi_y p_1 p_2^2 + \epsilon_{24} p_2^3, \\
R &= \epsilon_{34} p_2 + \epsilon_{35} p_1, \quad S = 2\epsilon_{16} p_1^2 + \eta_z p_1 p_2 + 2\epsilon_{26} p_2^2, \\
T &= \epsilon_x p_1^2 + \epsilon_y p_2^2 + \epsilon_z p_3^2.
\end{aligned}
\tag{B4}
$$

Note that for isotropic media, for which

$$
\epsilon_x = \epsilon_y = \epsilon_z = \frac{1}{2}\delta_x = \frac{1}{2}\delta_y = \frac{1}{2}\delta_z, \qquad \eta_x = \eta_y = \eta_z = 0, \tag{B5}
$$

and all other WA parameters are zero, see eqs (16) and (26) of Pšenčík & Farra (2005), we get in (B4): $A = B = ... = R = S = 0$. Only the term T remains non-zero in isotropic media. In this way, it is easy to check that all the expressions for the derivatives of $G(x_m, p_m)$ in eqs (B1) and (B2) reduce to exact ones for isotropic media.